We are IntechOpen, the world's leading publisher of Open Access books Built by scientists, for scientists

6,900
Open access books available

185,000
International authors and editors

200M
Downloads

Our authors are among the

154
Countries delivered to

TOP 1%
most cited scientists

12.2%
Contributors from top 500 universities



WEB OF SCIENCE™

Selection of our books indexed in the Book Citation Index in Web of Science™ Core Collection (BKCI)

Interested in publishing with us?
Contact book.department@intechopen.com

Numbers displayed above are based on latest data collected.
For more information visit www.intechopen.com



Chapter 10

Interfacial Tension and Contact Angle Data Relevant to Carbon Sequestration

Prem Bikkina and Imran Shaik

Additional information is available at the end of the chapter

http://dx.doi.org/10.5772/intechopen.79414

Abstract

Interfacial tension (IFT) between "native reservoir fluid" and "injected CO_2" and the contact angle (CA) among the reservoir rock, native reservoir fluid, and injected CO_2 are major factors that dictate the relative permeability and capillary pressure characteristics which in turn control the fluid flow and distribution characteristics in the reservoir and cap rocks. This chapter is a comprehensive review on the state-of-the-art of the experimentally measured and theoretically predicted IFT and CA data of water/brine-CO_2-quartz/calcite/mica systems that are relevant to CO_2 sequestration. Experimental techniques used to generate the IFT and CA data and details of molecular simulations used to predict the data are discussed. Respective comparisons of the IFT and CA data reported by various research groups are also made. Possible reasons for disagreements in the published literature are discussed, and suggestions are made for future research in this area to address the potential technical issues in order to obtain reproducible data.

Keywords: CO_2 sequestration, contact angle, interfacial tension, wettability, quartz, calcite, mica

1. Introduction

CO_2 (or carbon) sequestration is a process of injecting CO_2, that is typically captured at point sources such as coal gasification plants, and oil & gas production and refining facilities, into subsurface formations that have sufficient storage volume and stratigraphic confinement for it to be stored indefinitely to reduce its atmospheric concentration levels in order to mitigate the adverse effects of global warming [1–5]. Saline aquifers, depleted oil & gas reservoirs, and unminable coal seams are commonly considered host sites (shown in **Figure 1**) with

IntechOpen

© 2018 The Author(s). Licensee IntechOpen. This chapter is distributed under the terms of the Creative Commons Attribution License (http://creativecommons.org/licenses/by/3.0), which permits unrestricted use, distribution, and reproduction in any medium, provided the original work is properly cited. CC BY

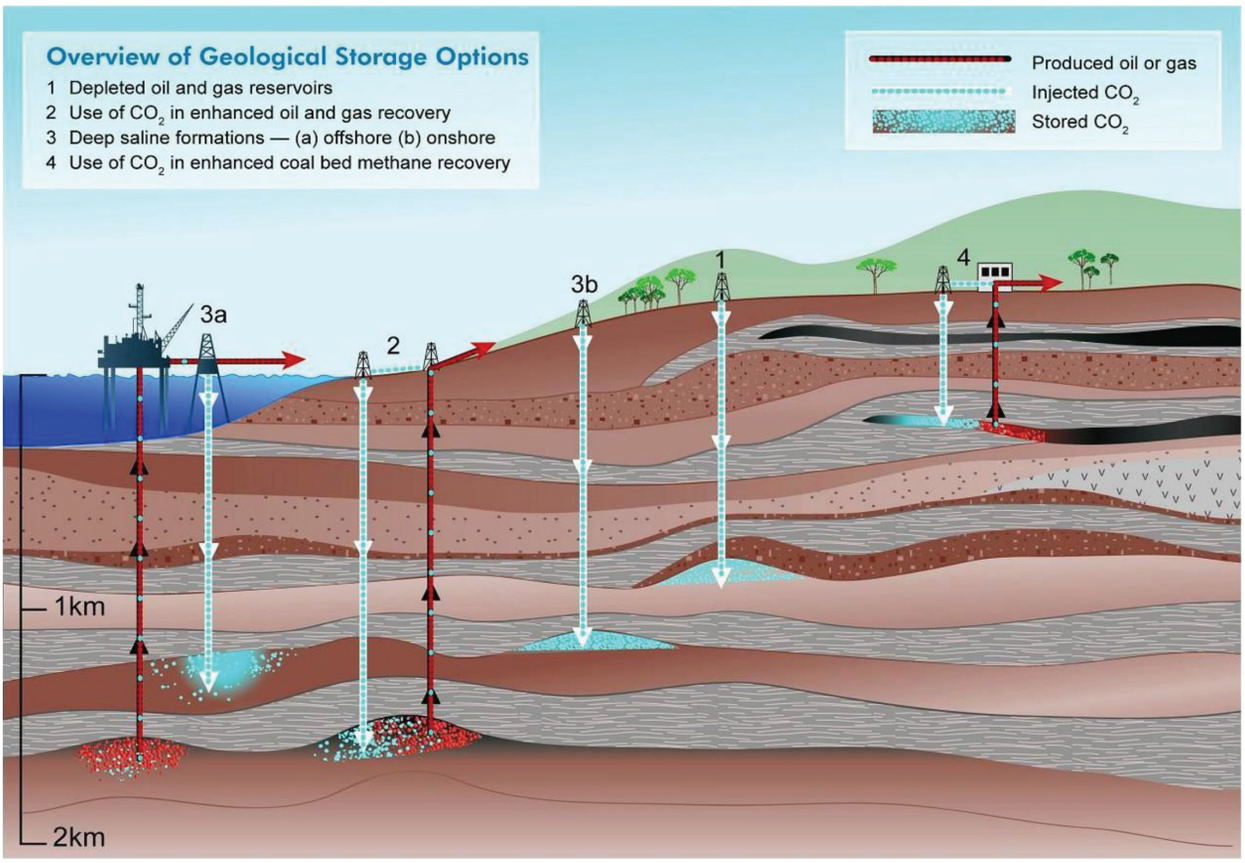


Figure 1. CO_2 sequestration methods (Source: SRCCS Figure TS-7, IPCC).

their respective advantages and disadvantages [6]. For example, saline aquifers are present in widespread areas so the CO_2 transportation cost is minimum but their storage and safety potentials are not well characterized, whereas depleted oil & gas reservoirs are well characterized but are scarcely present and hence the transportation cost from source to storage site is higher. CO_2 injection into oil & gas reservoirs and unminable coal seams may potentially recover enhanced oil and coalbed methane, respectively [6].

An ideal carbon sequestration site would consist of a reservoir rock with high porosity and permeability and a caprock with adequate sealing integrity. High porosity and permeability of the reservoir rock are important to have sufficient storage volume and efficient injection process, respectively. The low permeability caprock would facilitate the structural and stratigraphic confinement, which is a primary storage mechanism in the early years of the storage process, of the injected CO_2 [7].

Structural/stratigraphic trapping, residual/capillary trapping, solubility trapping, and mineral trapping are different types of trapping mechanisms for the injected CO_2. These trapping mechanisms are effective at various time scales during and after the injection process as shown in **Figure 2**. Structural/stratigraphic trapping is very critical during and in the first few years after the injection process. The injected CO_2 is normally lighter than brine or oil in the host site; hence, the buoyant force leads CO_2 towards caprock where it is stratigraphically

http://dx.doi.org/10.5772/intechopen.79414

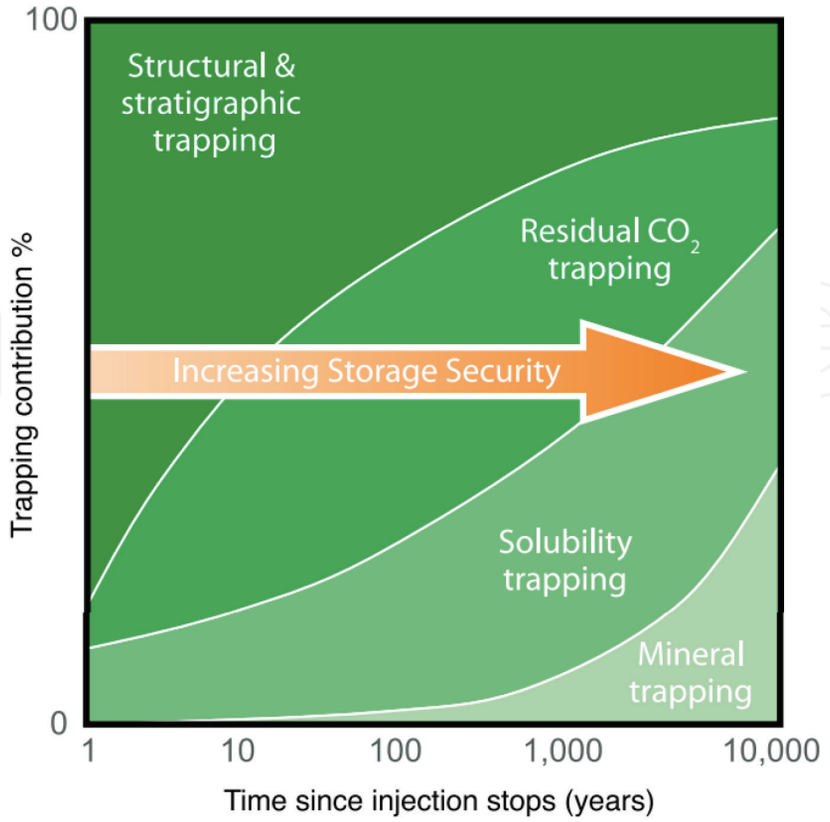


Figure 2. Post-injection contributions of CO_2 trapping mechanisms (Source: Figure 5.9 from IPCC 2005).

confined. During the injection process, CO_2 displaces the native reservoir fluid(s) (water and/or oil) and the displacement is usually a drainage process since CO_2 is usually the non-wetting phase (NWP). During injection, CO_2 moves forward and/or upward in the porous media, under the influence of positive capillary pressure (i.e., pressure in NWP–pressure in WP) and gravitational force, displacing the WP until irreducible wetting phase saturation ($S_{WP,\,r}$). After the injection is stopped (or pressure in NWP is reduced), WP moves back (imbibition) until the capillary pressure becomes zero. During the imbibition, WP displaces a fraction of the CO_2 while trapping the remaining fraction of the CO_2 as immobile disconnected ganglia [8]. This capillary immobilization of the CO_2 is termed as capillary or residual trapping. Later, portions of the immobile and mobile CO_2 dissolve in the native reservoir fluid(s), and the process is called solubility trapping [4]. The dissolved CO_2 reacts with minerals in the reservoir rock and forms solid carbonate minerals and is called as mineral trapping [4]. The percent trapping contributions of the four trapping mechanisms after the injection period are schematically shown in **Figure 2**.

The four trapping mechanisms, especially stratigraphic and residual trapping, are dependent on IFT and CA of the rocks and fluids involved [9]. The stratigraphic trapping depends upon the caprock's capillary entry pressure for CO_2. The capillary entry pressure is a function of the pore size, IFT between the native fluid (usually brine) in the caprock and injected CO_2, and relative wetting preference (CA) of the fluids to the caprock. The CA is the angle between the two tangent lines drawn at a point on three-phase contact line, one along fluid-fluid interface

and the other drawn along solid-fluid interface, as shown in **Figure 4(a)**, and is normally measured into the denser fluid phase. If the CA is higher than 90°, the rock has more preference to CO_2 compared to the native fluid, and hence it can easily imbibe into the caprock and leak through it. An ideal caprock for stratigraphic trapping would have strong wetting preference to native fluid (i.e. a CA value close to 0°).

Akbarabadi and Piri conducted 30 unsteady- and steady-state drainage and imbibition coreflooding tests in a medical CT scanner for CO_2-brine (10 wt.% NaI, 5 wt.% NaCl, and 0.5 wt.% $CaCl_2$) system in three different types of sandstone rock samples with 14.3–21.2% and 50–612 mD ranges of porosities and permeabilities [9]. They reported that at a given initial brine saturation (S_{wi}), less $scCO_2$ (11 MPa, 55°C) was trapped compared to gaseous CO_2 (3.46 MPa, 20°C) and the observed difference was attributed to brine being relatively less wetting to the rock in the presence of $scCO_2$. However, it should be noted that the above saturations were volume fractions and in terms of actual mass of the fluids trapped, $scCO_2$ is nearly 4 times higher than the gaseous CO_2. They also reported that about 49–83% of the initial CO_2 was capillary trapped during secondary brine imbibition. The influence of wettability on residual trapping of CO_2 was investigated by Rahman et al. [10]. They conducted microcomputed tomography (microCT) core-flooding experiments using 5 mm diameter and 10 mm length water-wet and oil-wet (originally water-wet sample was treated with 99.9 mol% purity Dodecyltriethoxysilane) Bentheimer sandstone samples having 22% porosity and 1800 mD permeability and CO_2-brine (7 wt.% NaI doped) fluid systems at 10 MPa and 318 K. The reported air-water CAs on the water-wet and oil-wet porous core samples were 0 and 130°, respectively. From the experimental findings, they concluded that lesser residual trapping occurs in oil-wet reservoirs (17.7% of initial CO_2) compared to water-wet reservoirs (29.4% of initial CO_2). The range of %capillary trapped CO_2 reported by Akbarabadi and Piri is much higher compared to the range reported by Rahman et al. [9, 10]. The difference in the %capillary trapped CO_2 ranges may be due to the differences in porosities and applied capillary pressures, as both the properties are known to affect the residual NWP saturation [8]. It should also be noted that the pore volumes of the core samples used by Akbarabadi and Piri [9] and Rahman et al. [10] were 24.1–36.3 cc and 0.044 cc, respectively.

Tokunaga et al. and Wang and Tokunaga conducted drainage and imbibition capillary pressure measurements for CO_2-brine (1 M NaCl) system in unconsolidated quartz [11] and limestone [12] sandpacks at 45°C and 8.5 and 12 MPa. The reported porosities of the sandpacks were ~38%. Based on the capillary pressure curves, they concluded that higher capillary trapping is possible for $scCO_2$ at higher pressures. The measured $S_{NWP,r}$ in both fresh and 1.5 months aged sandstone packs were 8% at 8.5 MPa, whereas the saturations for limestone sand were 11 and 25%. At 12 MPa, the measured $S_{NWP,r}$ in 3 months aged and 4.5 months aged sandstone packs were 20 and 32% and in fresh, 1.5 months aged, and 4 months aged limestone sand were 29, 25, and 44%, respectively. It should be noted that the above $S_{NWP,r}$ were measured at zero capillary pressure. By using capillary scaling criteria, they inferred that long-term (in the order of months) exposure of $scCO_2$ alters the wettabilities of the sands towards less brine-wet state.

For a safe and efficient sequestration process, an accurate representation of IFT and CA that strongly influence the relative permeability and capillary pressure is essential [13]. Further,

both IFT and CA data trends with pressure, temperature, and native and injected fluids compositions are of paramount importance during and post-injection periods [14]. Quartz/silica, calcite, and mica are dominant mineral species both in the reservoir and caprock systems; so, in this chapter, we review the current understanding on the effects of relevant process parameters on IFT and CA, the agreements and disagreements in the published data (both from the experimental and molecular simulation works), and potential reasons for the disagreements.

2. Measurement techniques

Sections 2.1 and 2.2 discuss key details of measurement techniques used for the IFT and CA data, respectively.

2.1. Interfacial tension

Drop shape analysis techniques (e.g., ADSA and ADSA-NA) that are suitable for direct measurement of IFT at high pressure and temperature conditions were used for most of the reported CO_2-water/brine IFT data [13, 15–28]. In general, the drop shape analysis methods involve: (1) formation of aqueous phase droplet in continuous CO_2 phase as shown in **Figure 3(a)** or CO_2 bubble/droplet in continuous aqueous phase as shown in **Figure 3(b)**, via a needle inside a pressure cell; (2) capturing the droplet image; (3) inputting the phase densities; and (4) obtaining IFT by matching the drop profile to the solutions of the Laplace equation [18, 25]. Capillary rise method was also used for the IFT data [29].

The following are the critical factors suggested to obtain reproducible IFT and/or CA data by: mutual saturation of the fluids and using saturated fluid densities [15]; placing thermocouple close to droplet phase [19]; avoiding contamination caused either due to low purity fluids and/or dissolution/rusting of wetted parts in fluids due to chemical incompatibility [30];

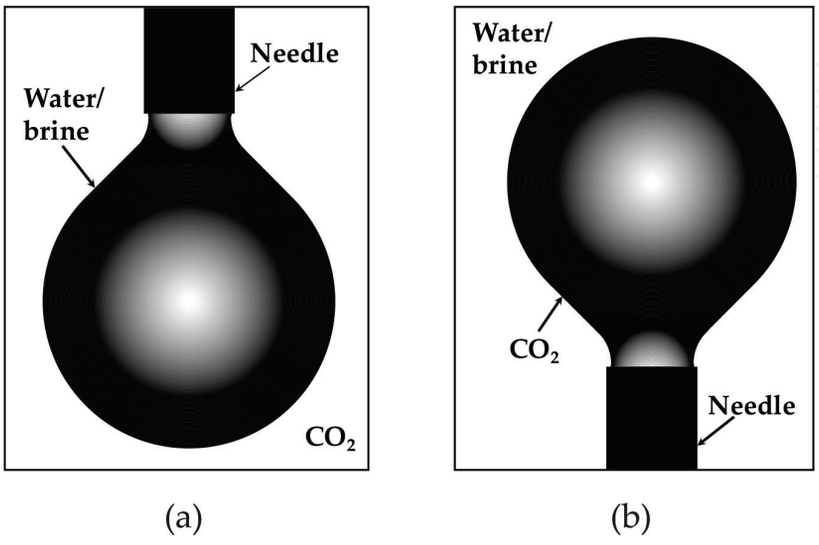


Figure 3. (a) Aqueous fluid droplet in CO_2 and (b) CO_2 bubble/droplet in aqueous fluid.

preventing droplet evaporation due to leakage of fluids and/or using unsaturated fluids [31]; and using same type of substrates with similar surface chemistry and morphology [32, 33].

2.2. Contact angle

Wettability of an inert solid surface is its relative affinity towards a fluid in the presence of another immiscible or sparingly soluble fluid. CA measurement is a widely used and accepted method for quantifying wettability of a surface. Direct and indirect measurement methods have been used for the published CA data [12, 16, 23, 31–38]. Direct methods include static

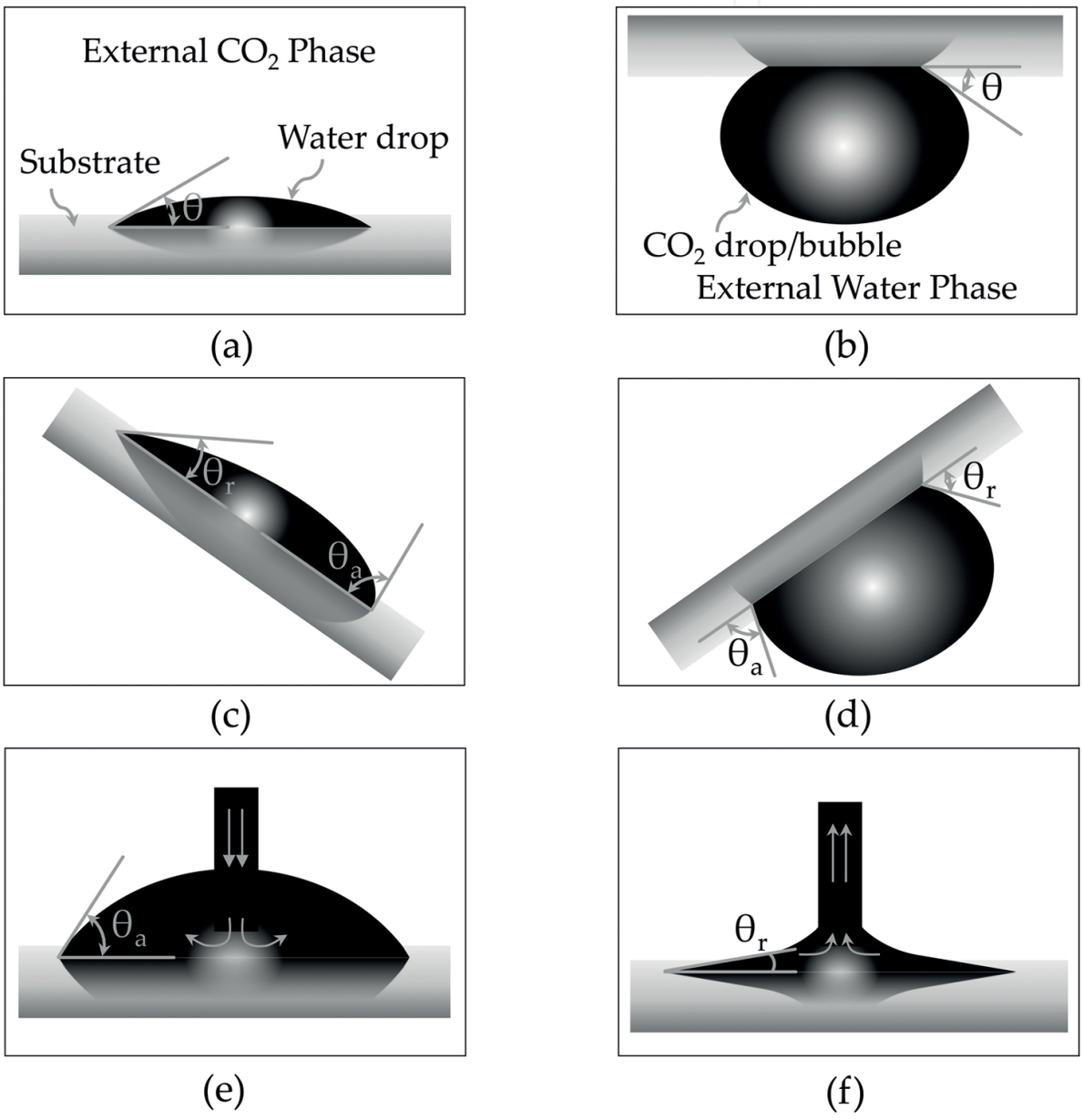


Figure 4. (a) Sessile aqueous fluid droplet on substrate in CO_2; (b) captive CO_2 bubble/droplet on substrate in aqueous fluid; (c) sessile aqueous fluid droplet on inclined substrate in CO_2; (d) captive CO_2 bubble/droplet on inclined substrate in aqueous fluid; (e) advancing aqueous fluid droplet on substrate in CO_2; and (f) receding aqueous fluid droplet on substrate in CO_2. Notation: θ—static CA; θ_a—aqueous fluid advancing CA; and θ_r—aqueous fluid receding CA.

(sessile-drop and captive-bubble) and dynamic (advancing and receding) CA measurements. Both the static and dynamic CAs were conducted using aqueous fluid as the droplet phase (called as sessile drop method, shown in **Figure 4(a)**) or the CO_2 phase as the bubble/droplet phase (captive bubble method, shown in **Figure 4(b)**).

For static CA measurement, the droplet phase is slowly released through a needle and deposited on the substrate immersed in external phase. In the case of advancing CA (w.r.t. droplet phase) measurement, either the droplet phase volume is slowly increased so that the three-phase contact line advances to an area where it was previously occupied by the external phase as shown in **Figure 4(e)** or the substrate is slowly titled so that the droplet phase advances on it due to gravitational or buoyant force. In the tilting base method, both the advancing and receding CAs can be measured simultaneously as shown in **Figure 4(c)** and **(d)**. Similarly, in the case of receding CA measurement, the droplet phase volume is slowly decreased so that the three-phase contact line recedes as shown in **Figure 4(f)**. CO_2 advancing (water/brine receding) CA is relevant for CO_2 injection into the reservoir and also to determine the capillary entry pressure of the caprock and thus to estimate the capacity of the host site to hold the injected CO_2. CO_2 receding (water/brine advancing) CA is required to estimate the amount of CO_2 that can be capillary trapped in the host site [39].

With the recent advancements in CT and microCT technologies, some researchers performed in-situ pore-scale CA measurements [37]. The procedure involves: (1) loading the core sample in an X-ray transparent coreholder; (2) scanning dry and wet core samples at various fluid saturations; (3) identifying rock and fluid phases in the collected tomographs; and (4) measurement of CA values either manually or using an automated algorithm.

CA data can be indirectly estimated from relative permeability or capillary pressure curves. Based on endpoint relative permeability of CO_2 in a core-flooding experiment where CO_2 displaces aqueous phase, relative wetting preferences of the fluids for the rock can be inferred. Typically, the endpoint relative permeability value less than 0.2 represents a strongly CO_2-wet porous media, whereas a value from 0.7 to 1 represents a strongly CO_2 non-wetting porous media. An endpoint relative permeability value close to 0.5 indicates an intermediate wetting state [36]. Advancing and receding CAs can also be estimated through capillary scaling of the drainage and imbibition capillary pressure curves [11, 12].

3. Fluids and substrate preparation methods

Sections 3.1 and 3.2 discuss the fluids and substrate preparation methods and their potential impact on the IFT and CA data.

3.1. Fluids

Various compositions of aqueous-rich phase and CO_2-rich phase fluids, ranging from pure water and CO_2 to brines containing different types of salts and salinities, and CO_2 streams with impurities such as H_2S, SO_2, N_2, and Ar have been used for both the published IFT and

CA data. The details of the compositions of the fluid phases, ranges of pressure and temperature, whether the fluids had been mutually saturated before the IFT and CA measurements, whether the saturated fluid phase densities were used for the IFT measurement, and how the phase densities were obtained are provided in **Table 1**.

3.2. Substrates

Quartz is one of the polymorphs of silica (SiO_2). The other polymorphs include tridymite, cristobalite, coesite, stishovite, etc. There are two types of quartz based on the geometrical positions of the atoms: α-quartz and β-quartz [51]. The published CA data were collected on α-quartz as it is related to typical pressure and temperature ranges of CO_2 sequestration. Calcite and aragonite are the two polymorphous groups of carbonate minerals. Calcite ($CaCO_3$) is a mineral in calcite group. Generally, these minerals are impure, but majority of the CA data were collected on Iceland Spar calcite crystals which are pure $CaCO_3$ [33, 34, 52]. Mica group is a subdivision of phyllosilicates. Muscovite ($KAl_3Si_3O_{10}(OH)_2$), also known as common mica or potash mica, is the most common form of mica. Phlogopite ($KMg_3(AlSi_3O_{10}(OH,F)_2$), called as Mg-Mica, is another form of mica. Mica is usually soft and has perfect basal cleavage [53]. Both muscovite [27, 35, 40, 54, 55] and phlogopite [34] micas have been used for CA data related to carbon sequestration.

In a short communication, Iglauer et al. attempted to identify possible reasons for the observed scatter in the reported CA data of quartz/glass-CO_2-water/brine systems [30]. Different cleaning procedures such as acetone washing followed by DI water rinsing, piranha solution (5:1 v/v H_2SO_4 and H_2O_2) cleaning (etching), and air plasma cleaning were evaluated. Approximately 0° CAs on the surfaces cleaned using piranha solution and air plasma were reported. It was also reported that the CA of piranha solution cleaned substrate increased to about 25° when a clean paper towel was used to wipe the substrate and to 70° when the substrate was kept in the laboratory atmosphere for several weeks. Even though both the piranha solution and plasma cleaning could give near 0° CA, plasma cleaning was suggested based on its relative merits in terms of health and environmental hazards. However, there is a significant scatter in the CA data of plasma cleaned quartz/silica surfaces. For example, water advancing CAs reported for Ar plasma and 20% O_2–80% Ar plasma cleaned quartz surfaces were 40 and 16°, respectively [56]. The publication also reported advancing and receding CAs of about 39 and 23° for piranha solution cleaned quartz surface. Another study reported an air-water CA of about 45° on silica that had been cleaned using reactive ion etching oxygen plasma [57].

As Iglauer et al. [30] pointed out, surface contamination is one of the critical factors that affects wettability of a substrate; however, severe surface cleaning methods such as plasma or piranha etching could also alter the surface chemistry and/or morphology both of which are known to modify the wettability of a substrate [58, 59]. Quartz/silica surface cleaning has been done using degreasing chemicals such as acetone, methanol, and trichloroethylene and strong oxidizing agents such as hot nitric acid, hydrogen peroxide, and hydrofluoric acid that may remove surface layer [56].

Author (Year)	Aqueous-rich phase	CO_2-rich phase	P (MPa)	T (K)	Pre-equilibrated?	Densities for IFT	Cleaning chemicals
Chun et al. (1995) [29]	DIW	CO_2	0.1–18.6	278–344	No	Water: NM, CO_2: Pure	NM
Chiquet et al. (2007) [18]	0–0.34 M NaCl	CO_2	5–48	308–383	Yes	DM	C: NM
Chiquet et al. (2007) [55]	0.01–1 M NaCl	CO_2	1–11	NM	No	NA	S: TND
Bachu et al. (2008) [20]	0–5.72 M NaCl	CO_2	2–27	293–398	Yes	DM	NM
Shah et al. (2008) [21]	Water	CO_2:H_2S, 70:30 mol%	0.45–15.6	313–393	Yes	Water: PRSW, CO_2: PRSW	NM
Chalbaud et al. (2009) [13]	0–2.75 M NaCl	CO_2	4.5–25.5	300–373	Yes	Brine: SWRC, CO_2: Pure	C: DIW
Espinoza et al. (2010) [23]	0–3.42 m NaCl	CO_2	0.1–20	296.5 ± 1.5	No	Brine: PGM, CO_2: DS	NM
Georgiadis et al. (2010) [24]	DIW	CO_2	1–60	298–374	No	NIST	C: HITC
Aggelopoulos et al. (2011) [22]	0.045–1.5 M NaCl: $CaCl_2$, 50:50 mol%	CO_2	5–25	300–373	Yes	Brine: SWRC, CO_2: Pure	C: EDC
Bikkina et al. (2011) [15]	DIW	CO_2	1.48–20.76	298–333	Yes	Water: HB, CO_2: MS	C: ADC
Bikkina (2011) [31]	DIW	CO_2	1.48–20.76	298–323	Yes	NA	C: AD, Quartz: AD, Calcite: DIW
Broseta et al. (2012) [40]	0.08–6 M NaCl	CO_2	0.5–15.5	282–413	Yes	NA	NM
Jung et al. (2012) [41]	0–5 M NaCl	CO_2	0.1–25	318	Yes	NA	C: DIW, S: Ethanol
Shariat et al. (2012) [25]	DIW	CO_2	6.89–124.1	323–478	No	BM	NM
Farokhpoor et al. (2013) [35]	0–0.8 M NaCl	CO_2	0.1–40	309–339	No	NA	S: DDN C: WMC
Saraji et al. (2013) [16]	DIW	CO_2	3.45–11.72	308–333	Yes	DM	S: IHND

Author (Year)	Aqueous-rich phase	CO_2-rich phase	P (MPa)	T (K)	Pre-equilibrated?	Densities for IFT	Cleaning chemicals
Iglauer et al. (2014) [30]	0–0.342 M NaCl & 1 M $NaHCO_3$	CO_2	0.1–13.89	296–323	No	NA	Piranha solution or air plasma
Saraji et al. (2014) [42]	0.2–5 M NaCl	CO_2 + SO_2 (0–6 wt%)	13.89–27.68	323–373	Yes	DM	S: IHND
Al-Yaseri et al. (2015) [26]	0.084 M NaCl	CO_2 + N_2 (0–50 mol%)	13	333	No	GS	S: Acetone and air plasma
Arif et al. (2016) [27]	0–5.13 M NaCl	CO_2	0.1–20	308–343	No	NM	S: Air plasma for 45 min
Kravanja et al. (2018) [28]	0.3 M Brine*	CO_2 + Ar (0–100 vol%)	0.1–40	313–363	Yes	DM	NM

DIW: DI water; C: cell; S: substrate; NM: not mentioned; NA: not applicable; DM: Anton Paar DMA density meter; PRSW: Peng and Robinson [43] and Søreide and Whitson [44]; SWRC: Søreide and Whitson [44] and Rowe and Chou [45]; PGM: Perry and Green [46] and McCutcheon et al. [47]; DS: Duan and Sun [48]; NIST: National Institute of Standards and Technology Chemistry Webbook; BM: Blue M Model CSP-400A; HB: Hebach et al. [49]; MS: modified Spycher et al. [50]; GS: from Georgiadis et al. [24]; TND: tensioactive solution, 10% nitric acid solution and DI water; HITC: hexane, isopropanol, and/or toluene, CO_2 flush; KID: KOH-isopropanol solution and DI water; CNE: cyclohexane, nitrogen, and ethanol; EDC: ethanol, DI water, and CO_2; ADC: acetone, DI water, and CO_2; DA: DI water and acetone; DDN: DI water, Deconex, and 6% nitric acid solution; WMC: water, methanol, and dry CO_2; IHND: IPA, H_2SO_4 with 10% Nochromix, DI water [43–50].*(10.88 g/L KCl, 6.68 g/L $NaHCO_3$, 3.14 g/L NaCl, and 2.38 g/L K_2CO_3).

Table 1. Details of fluids, process conditions, and cleaning chemicals used for published IFT and CA data.

Iglauer et al. concluded that a clean quartz/silica surface should have a 0° air-water CA; however, since the wettability of quartz/silica is primarily determined by surface silanol (Si-OH) group density that could vary from a sample to sample, the CA does not necessarily be 0° [30, 60, 61]. For example, as reported in [58], even a freshly prepared silica surface has an air-water CA of about 45°. The publication also mentions that cleaning methods such as acid washing would hydroxylate the surface and correspondingly reduce the CA (or make it hydrophilic). Suni et al. mentioned that plasma treatment induces a highly disordered surface structure and significantly increases the surface silanol group density [59]. Lamb and Furlong reported that when the surface silanols on a quartz substrate are changed to siloxane (Si-O-Si) bridges, the substrate becomes less water-wet with an advancing CA of 44° and a receding CA of 39° [60].

Quartz, calcite, and mica substrates used for published CA data have many orders of magnitude difference in their surface roughness values. For example, quartz and calcite substrates with surface roughness values ranging from 0.5 to 1300 nm [16, 32, 34, 38] and 7.5 to 250 nm [33, 34], respectively, were used for the CA measurements. CA values are known to be affected by the surface roughness values and cleaning methods [32, 33, 56, 62]. The trends of the effect of surface roughness on CAs measured on quartz and calcite substrates are discussed in CA data comparison section.

http://dx.doi.org/10.5772/intechopen.79414

4. Theoretical studies on IFT and contact angle data

Molecular dynamics simulations for the prediction of IFT and CA data were performed by various research groups for systems pertaining to CO_2 sequestration [19, 63–70]. The simulation procedure consists of choosing potential models for molecules, intermolecular interaction models for short-range and/or long-range interactions, initial and boundary conditions, and the ensemble (NVE, NVT, NPT, etc.), followed by simulation until equilibration criteria is satisfied. After simulation, the results (IFT/CA data) are analyzed and compared with experimental values. The models evaluated were CO_2—DZ, EPM2, flexible EPM2, PPL and TraPPE; Water—SPC, SPC/E, TIP4P2005, F3C, and flexible F3C; and NaCl brine—SD and DRVH [19, 63, 64, 66, 68].

The predictions on the effect of temperature and pressure on IFT for CO_2-water system were found to be in good agreement with experimental data for the models used by Nielsen et al. (PPL-TIP4P2005 and renormalized PPL-SPC/E) and Liu et al. (TraPPE-TIP4P2005 (and SD model for NaCl) below 250°C except at 150°C and EPM2-SPC at 150°C), whereas EPM2-TIP4P2005 model combination used by Iglauer et al. and Liu et al. resulted in overprediction of IFT [64–66]. EPM-SPC/E model combination used by Kvamme et al. and Nielsen et al. underpredicted IFT data in the low-pressure region (<4 MPa) and overpredicted in the high-pressure region (>10 MPa) [19, 65]. Nielsen et al. [65] observed the similar trend for DZ-SPC/E model combination, and they also observed that PPL-SPC/E model combination underpredicted IFT throughout 0–40 MPa. In agreement with experimental data [20, 22, 41, 42], IFT was found to increase with salinity by Zhao et al., Iglauer et al., and Liu et al. [63, 64, 66].

Various research groups performed CA predictions for water/brine–CO_2–quartz/silica systems using molecular dynamics simulations [64, 67, 69, 70]. Iglauer et al. and McCaughan et al. considered fully coordinated quartz (i.e., siloxane bridges (Si-O-Si) and no silanol groups) surface structure and they only used short-range force field parameters Si-O (bonded) and O-O (non-bonded) retrieved from Beest and Kramer [64, 67, 71] in their simulations. Iglauer et al. [64] reported an abrupt increase in CA (0–80°) for water-CO_2-quartz system at 300 K in the low-pressure region (0–6.7 MPa) and a nearly constant CA above 6.7 MPa. Simulations performed by McCaughan et al. [67] for 1 M $CaCl_2$ brine-CO_2-quartz system at 300 K yielded similar CA values with pressure showing negligible effect of the divalent ions. At 350 K, significantly smaller CA values near both sides of the phase changing pressure were reported by Iglauer et al. [64] and the CA values at pressures above 17 MPa were found to be identical for 300 and 350 K. They also reported no significant effect of salinity (1 and 4 m NaCl) on CA at 300 K and ~4 MPa.

Liu et al., McCaughan et al., and Chen et al. considered hydroxylated quartz surfaces with different silanol group densities ranging from 1.6 to 9.4 OH/nm^2 for CA measurements [67, 69, 70]. Liu et al. [70] modeled a pristine silica plane having silicon atoms on the surface as hydrophobic surface and its partially hydroxylated variant with a silanol density of 1.6 OH/nm^2 as hydrophilic surface. They reported that CA on the hydrophilic surface increased from ~60 to ~90° when the CO_2 density increased from 0 to 1 g/cc. In the case of hydrophobic surface, water droplet with a CA of 115° at

0.2 g/cc CO_2 density lost its contact from the surface upon further increase in CO_2 density. At 300 K and 10 MPa, McCaughan et al. [67] reported that the CA reduced with increasing silanol group density (42° at 1.7 OH/nm^2 to 35° at 3.7–4.5 OH/nm^2). Chen et al. [69] performed molecular simulations, on fully hydroxylated silica surface with 9.4 OH/nm^2 silanol group density, using force field parameters for Si-O, O-H, O-Si-O, Si-O-Si, and Si-O-H groups to predict CAs for brine-CO_2-quartz systems. 0–3 M NaCl and $CaCl_2$ brines were used in the study. The predicted static CAs (e.g., 22.6° for water) agreed well with their experimental results (20–21°). Their results indicate that CA slightly increases (about 7–13°) with ionic strength (0–3 M), and the trend is similar for both monovalent and divalent ions. They also reported that CA dependence on pressure and temperature is insignificant within the conditions tested (7 and 9.6 MPa at 318 K and 10.9 MPa at 333 K).

Tenney and Cygan performed molecular dynamics simulations for brine-CO_2-clay system at 330 K and 20 MPa and reported CO_2 CAs for hydrophilic gibbsite and hydrophobic siloxane surfaces in the presence of water, NaCl, and $CaCl_2$ brine solutions. The reported CO_2 CAs were 169° in water and 180° in both brines on the hydrophilic surface, whereas on the hydrophobic surface, the reported CO_2 CAs were 145° in water, 141° in 0.78 M NaCl brine, and 145° in 0.26 M $CaCl_2$ brine [68].

5. Interfacial tension data comparison

There have been a significant number of experimental and simulation studies on the IFT data of CO_2-water/brine systems at typical reservoir pressure and temperature conditions. In general, a fair agreement in the trends and values can be observed in the data reported by various research groups [15, 20, 28, 29, 72]. **Figure 5** shows reproducibility of the effect of pressure on IFT data for CO_2-water system at 298 K.

As shown in **Figure 5**, IFT sharply decreased with pressure when the CO_2 is gas and it becomes nearly constant when the CO_2 is liquid. It should be noted that Hebach et al., Bachu and Bennion, Bikkina et al., and Kravanja et al. used pendant drop method, whereas Chun et al. used capillary rise method [15, 20, 28, 29, 72]. The lowest IFT reported by Chun et al. [29] near the phase changing pressure was explained by Hebach et al. [72] as a potential consequence of the placement of thermocouple away from the droplet.

Similarly, IFT vs. pressure trends were also observed at above critical temperature of CO_2-rich phase, as shown in **Figure 6** [15]. Majority of the reported experimental and molecular simulations IFT data for CO_2-water system show an increase in IFT with temperature when the CO_2-rich phase is gas and the temperature is above the critical temperature and when CO_2 is gaseous phase [15–17, 20, 24, 29, 64, 72]. The increase in IFT with temperature is higher near the phase changing pressure from gaseous to supercritical CO_2. At very low pressures (of about 2.5 to 3.5 MPa), the IFT vs. temperature isotherm crossover was reported by Hough et al. [17], Chun et al. [29], and Hebach et al. [72], but Hebach et al. [72] hypothesized that the observed crossover of the isotherms could be due to the use of pure component phase densities instead of saturated phase densities for CO_2 and water. Bikkina et al. [15] used saturated phase densities for their IFT data and did not observe the crossover point to a pressure as low

http://dx.doi.org/10.5772/intechopen.79414

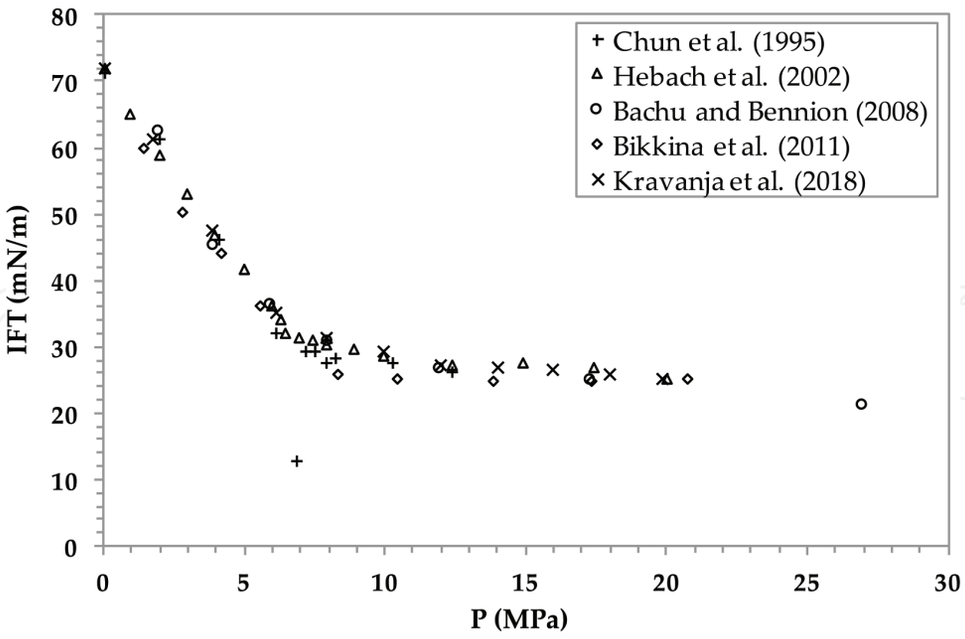


Figure 5. Comparison of published IFT data for CO_2-water system at 298 K [15].

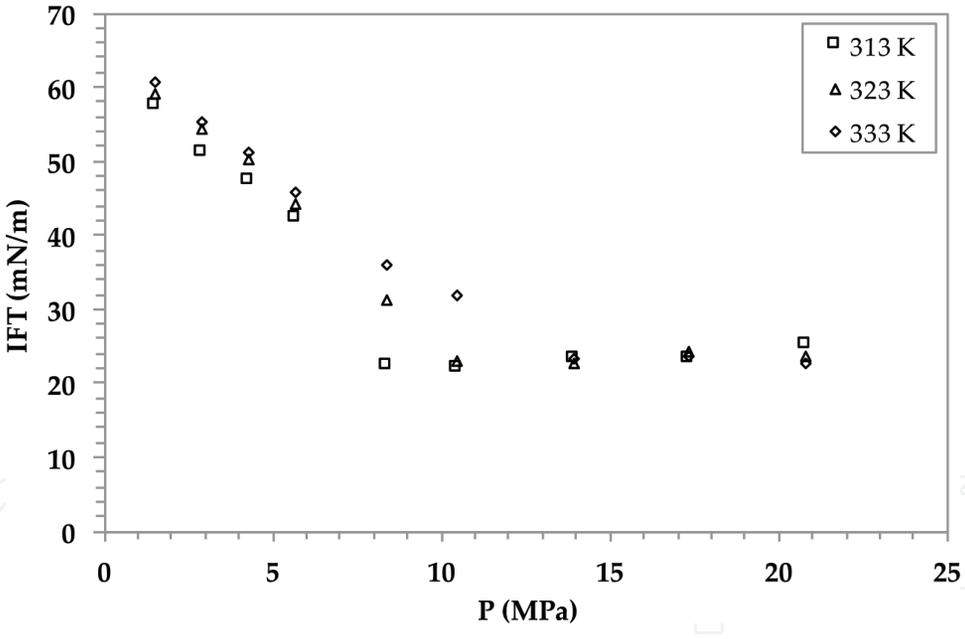


Figure 6. IFT isotherms for the CO_2-water system at various pressures [15].

as 1.48 MPa, as shown in **Figure 6**. For pressures above ~13 MPa and temperatures above the critical temperature (i.e., supercritical state), no or insignificant effect of temperature on IFT was reported [15, 17, 29, 64, 65, 72]. Whereas, a decrease in IFT with temperature between 212 and 400°F and pressure up to 18,000 psia was reported by Shariat et al. [25]. It should be noted that the experimental temperatures used for Shariat et al. [25] data are much higher than others.

As shown in **Figure 7**, an invariant IFT vs. "aqueous and CO_2 phase density difference ($\Delta\varrho$)" irrespective of the pressure and temperature until a $\Delta\varrho$ of about 600 kg/m^3 and then a steep increase in IFT with $\Delta\varrho$ was reported by Bikkina et al. [15]. Similar trends were reported by Chalbaud et al. for CO_2-NaCl brine system [13].

There has been a common agreement on the effect of salinity on IFT data (from experimental measurements and molecular simulations) of CO_2-brine systems [13, 15, 20, 22, 42, 63–65]. At a given pressure and temperature condition, IFT was observed to increase with salinity. Aggelopoulos et al. [22] reported that the increase in IFT, at a given molality of aqueous phase, is more than double for $CaCl_2$ solution compared to that of NaCl solution reported by Chalbaud et al. [13], and this increase was attributed to the presence of divalent cations in the case of $CaCl_2$ solution.

The influence of H_2S, SO_2, N_2, and Ar contamination in CO_2 stream on IFT were investigated by Shah et al., Saraji et al., Al-Yaseri et al., and Kravanja et al., respectively [21, 26, 28, 42]. Shah et al. [21] conducted water-H_2S IFT measurements up to 15 MPa and at 120°C and water-(30, 70 mol% H_2S:CO_2) IFT measurements up to 15 MPa and at 77°C. Upon combined analyzation of their IFT data along with Chiquet et al. [18] water-CO_2 IFT data, they concluded a strong decrease of IFT with increase in H_2S content in CO_2. A significant linear decrease in IFT (i.e. from 29 mN/m in the case of pure CO_2 to 18 mN/m in the presence of 6 wt% SO_2) was reported by Saraji et al. [42]. The presence of weakly bounded surface complex between SO_2 and water molecules at the supercritical fluid/liquid interface was suggested as the probable reason for the decrease in IFT. Pressure, temperature, and salinity conditions used in their experiments were 3000 psig, 60°C, and 1 M brine, respectively.

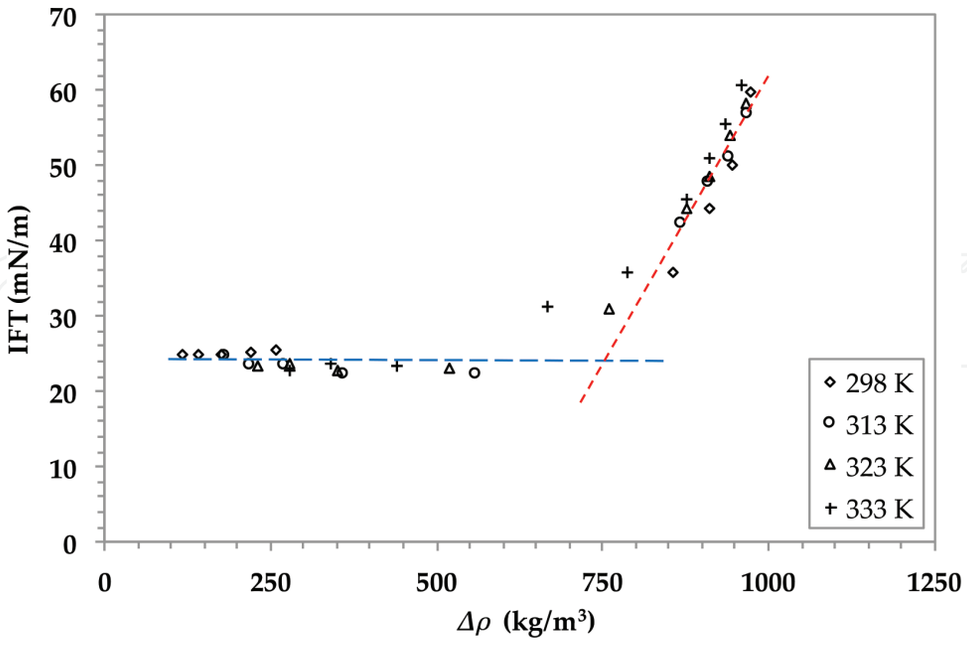


Figure 7. Effect of phase density difference on IFT for the CO_2-water system at various temperatures [15].

Effect of N_2 contamination on IFT was studied by Al-Yaseri et al. [26]. About 5000 ppm NaCl brine and 50:50 mol% CO_2-N_2 mixture were used as aqueous and gas phases, and the IFT measurements were conducted at 13 MPa and 333 K. It was found that 50 mol% N_2 has negligible effect on IFT (CO_2-brine IFT of 38.7 ± 3.9 mN/m and 50:50 mol% CO_2/N_2 mixture-brine IFT of 40.6 ± 3 mN/m) within experimental uncertainty. Kravanja et al. [28] measured IFT between CO_2 stream containing Ar impurity and 23.26 g/L salinity brine and found that the presence of 5 and 10 vol.% Ar impurity in CO_2 stream has negligible effect on IFT within the temperature and pressure ranges of 40–90°C and 7.5–40 MPa.

6. Contact angle data comparison

There is a significant scatter in the reported CA (wettability) data [30, 54]. The reported CA data include static [23, 30, 31, 41] and dynamic [16, 27, 30, 32, 33, 35, 38, 42, 55] CAs. The data also include measurements of water/brine droplet on substrate in CO_2 [23, 26, 27, 30, 31, 33, 38, 41] and CO_2 bubble/droplet on substrate immersed in aqueous phase [34, 35, 41, 42, 54, 55]. One of the major reasons for the apparent spread in CA data is in fact due to the comparison of the data collected at significantly different process parameters. For example, the CA data collected on quartz substrates having orders of magnitude, different surface roughness values, and at different temperatures and salinities were compared [38]. Similar inappropriate comparisons were also made for calcite [33] and mica substrates [27]. It should also be noted that even static and dynamic CAs have been compared [27, 33].

It is possible that the so-called smooth and pure substrates used for some of the published data may have surface chemical and physical heterogeneity which could cause significant CA hysteresis (i.e., the difference between advancing and receding CAs). In general, static CA falls somewhere between the advancing and receding CAs [73]. Hence, it is inappropriate to compare static and dynamic CAs. Some researchers reported surface roughness data of their substrates [16, 27, 32–34, 38, 41, 42, 74]. The reported quartz surface roughness data range from 0.5 to 1300 nm (5 orders of magnitude). In the case of mica, Wang et al. [34] used phlogopite mica with 250 nm surface roughness and Arif et al. [27] used muscovite mica with a roughness value of 12 nm.

Al-Yaseri et al. thoroughly investigated the influence of surface roughness on advancing and receding CA trends of quartz-CO_2-water system using the substrates of different surface roughness (RMS) values: 56, 210, 560, and 1300 nm [32]. They found that as the roughness increases from 56 to 1300 nm, advancing and receding CAs at 296 K and 10 MPa decrease by ~6.5 and ~2°, respectively, whereas at 323 K, the CAs decrease by ~14 and ~14°, respectively. The effect of surface roughness on advancing and receding CA trends of calcite-CO_2-water system was studied by Arif et al. using calcite substrates of surface roughness (RMS) values: 7.5, 30, and 140 nm [33]. They noted that as the roughness increases from 7.5 to 140 nm, both the advancing and receding CAs at 323 K and 15 MPa decrease by ~10°. There have not been any systematic experimental studies reported on the influence of surface roughness on CA of mica-CO_2-water system.

Al-Yaseri et al. and Arif et al. measured advancing and receding CAs on quartz and calcite substrates placed on 12° and 15° (w.r.t horizontal) tilted bases, respectively. About a 6 μl water droplet that was not pre-saturated with CO_2 was dispensed on to the titled substrate and the advancing and receding CAs were measured on droplet images extracted from the recorded video [32, 33].

Al-Yaseri et al. [32], Arif et al. [27], and Arif et al. [33] also investigated the effect of pressure, temperature, and salinity on advancing and receding CAs of quartz-CO_2-water, mica-CO_2-water, and calcite-CO_2-water systems, respectively. The pressure, temperature, and salinity ranges studied for quartz, mica, and calcite substrates were: 0.1–20 MPa, 296–343 K, and 0–35 wt% (NaCl, $CaCl_2$, and $MgCl_2$); 0.1–20 MPa, 308–343 K, and 0–30 wt% NaCl; and 0.1–20 MPa, 308–343 K, and 0–20 wt% NaCl, respectively. For both quartz and calcite substrates, advancing and receding CAs increased with pressure, but the effect of temperature was different for the substrates. Both the advancing and receding CAs increased with temperature in the case of quartz, but the opposite trend was reported for calcite. In the case of quartz, both the advancing and receding CAs increased with salinity and the increase was higher for $MgCl_2$, followed by $CaCl_2$ and NaCl. Whereas in the case of calcite, salinity has negligible effect on both the advancing and receding CAs up to 5 wt% NaCl and the CAs increased with salinities above 5 wt% NaCl. The effect of pressure and temperature on advancing and receding CA trends of mica was similar to that of calcite. The effect of salinity on mica CA was similar to that of quartz.

Broseta et al. conducted water/brine advancing and receding CA measurements on quartz, calcite, and mica substrates [40]. For quartz, insignificant change in receding CAs with pressure (0.5–14 MPa) and salinity (0.08–6 M NaCl) was observed, whereas increase in the advancing CAs with the pressure and salinity was reported. For calcite, the receding and advancing CAs increased by 8 and 15°, respectively, with pressure (0.5–14 MPa) at 0.08 M and 308 K. In case of mica, the change in receding CAs with pressure was less than 10°, but a significant increase (up to ~40°) in advancing CAs with pressure was observed when there was CO_2 adhesion to mica. However, when there was no CO_2 adhesion, the increase in advancing CAs with pressure was only about 10°. Wan et al. also observed CO_2 adhesion on mica and similar levels of hysteresis in CA; however, they did not observe any clear CA trends with pressure and salinity [54].

Espinoza and Santamarina [23] and Bikkina [31] measured static CAs by placing a single aqueous fluid droplet on substrate (quartz/calcite) at a given temperature and pressure and successively injected CO_2 into the measurement cell to increase the system pressure. For quartz substrate at 298 K (below critical temperature of CO_2, $T_{c,CO2}$), they did not observe any significant effect of pressure on CA, both in gaseous and liquid regions; however, the values reported by Espinoza and Santamarina [23] and Bikkina [31] were ~20 and ~45°, respectively. At 313 and 323 K (i.e., above $T_{c,CO2}$), Bikkina [31] observed about 5° increase in CA in gaseous region compared to 298 K and the CA gradually decreased in supercritical region. The surface roughness values of the substrates used were not reported in both the above studies. Bikkina [31] used equilibrated fluids and the droplet was placed on the substrate at 1.48 MPa, whereas Espinoza and Santamarina [23] used non-equilibrated fluids and the

droplet was placed at 0.1 MPa. Bikkina [31] reported a significant shift in CA towards less water-wet state upon repeated exposure of the substrates to liquid or $scCO_2$. Desorption of physisorbed water and subsequent capping of the silanols (on quartz surface) by CO_2 were proposed as the possible mechanism for the observed CA shift, and hence the CA measurement systems with CO_2 as droplet phase may not observe this phenomenon due to insufficient CO_2 volume [75]. Kim et al. (2012) observed a dewetting phenomenon in brine-filled silica micromodels upon exposure to $scCO_2$. The tested pressure, temperature, and salinities were 8.5 MPa, 318 K, and 0.01–5 M NaCl. The pore-scale CAs were observed to increase from near 0 to 80° upon exposure to $scCO_2$, and the highest CA increase was observed in the case of 5 M brine [76].

For calcite substrate, at ~298 K, both Espinoza and Santamarina [23] and Bikkina [31] reported a sudden dip (~6°) in the CA at the phase changing pressure. The CA values reported by Bikkina [31] were 45–48° in CO_2 gaseous region and 42–40° in the CO_2 liquid region. The corresponding values reported by Espinoza and Santamarina [23] were 35 and 30°, respectively. Andrew et al. performed pore-scale CA measurements for CO_2-brine-carbonate (99.1% calcite and 0.9% quartz) system at 10 MPa and 323 K, after secondary imbibition. The observed CA values were in the range of 35 and 55° [37].

Wang et al. [34] reported CAs of dissolving CO_2 bubble/droplets as water/brine advancing CAs, so it appears that the CAs are neither static nor dynamic. It should be noted that the dissolution occurred irrespective of using pre-equilibrated fluids. If there exists evaporation/dissolution of the droplet, the corresponding CA can increase, decrease, or stay constant depending upon the relative molecular forces among the three phases involved and the triple line movement [77–79]. Farokhpoor et al. [35] reported that water/brine receding CAs on quartz and calcite and no significant effect of pressure on the CAs were observed. They reported increase in CAs with temperature and salinity for quartz substrate, but a decrease in CA with salinity for calcite substrate.

Three significantly different CA trends with pressure have been reported for quartz/silica: (1) no or insignificant change in CA [23, 31, 35, 69]; (2) sudden increase in CA near the phase changing pressure [40–42]; and (3) asymptotic increase in CA with increase in pressure [32, 64]. Al-Yaseri et al. found a remarkable linear correlation between CA and density of gas for quartz-brine (4.48 M = 20 wt% NaCl +1 wt% KCl) system [80]. The correlation is applicable for a wide range of gases. Temperature was found to change the slope of the correlation.

Saraji et al. [42] studied the influence of SO_2 contamination in CO_2-rich phase on advancing and receding CAs (using drop addition and withdrawal method) on quartz at 3000 psig, 60°C, and 1 M NaCl. They observed insignificant difference in the CAs with 1 and 6 wt% SO_2 compared to those measured for pure CO_2 at the same pressure, temperature, and salinity. Effect of N_2 contamination on water advancing CA on quartz was studied by Al-Yaseri et al. [26] using drop addition method. About 5000 ppm NaCl brine and 50:50 mol% CO_2:N_2 mixture were used as aqueous and gas phases, and the CA measurements were conducted at 13 MPa and 333 K. They reported 47 ± 3.4°, 33.9 ± 6°, and 40.6 ± 3.9° water advancing CAs for CO_2-brine, 50:50 mol% CO_2:N_2 mixture-brine, and N_2-brine systems, respectively.

7. Recommendations for future work

We believe that the potential reasons for the scatter in the CA data are due to the differences in: substrate types used (e.g., muscovite mica and phlogopite mica, quartz and silica), their preparation methods, and surface roughness values and patterns; fluid types (i.e. purities of droplet and external phase fluids and whether the fluids had been mutually saturated in the presence of substrate material); chemical compatibility of the materials used in the experimental facilities with the cleaning and process chemicals; types of CA data reported (e.g., static or dynamic CAs, sessile or captive, one droplet/bubble for a given pressure range or new droplet/bubble at each pressure). Repeatability in the data is necessary but not sufficient. Reproducibility is what is important. So, comparisons should only be made among the data collected using same system of solid and fluids, purities and preparation methods, measurement techniques, and especially type of CA data. We suggest microCT-based in-situ CA measurement with automated three-phase contact line detection for simultaneously obtaining several hundreds of thousands of CA values, as performed by AlRatrout et al. [81]. The method may also provide relative permeability and capillary pressure data for indirect estimation of wettability. One disadvantage of the suggested method is the requirement of doping the fluids. We also suggest in-situ surface chemical analysis as performed by Tripps and Combs [75] during the CA measurement in order to know any surface chemical alterations responsible for CA changes.

8. Conclusions

A detailed overview on the published IFT and CA (experimental and molecular simulation) data relevant to CO_2 sequestration is presented. Overall, the IFT trends reported by various research groups are found to be in good agreement, but there exists significant scatter in the reported CA data. Potential reasons for the disagreements in CA data are discussed, and recommendations are made for future research to obtain reproducible CA data.

Acknowledgements

The authors convey their sincere gratitude to Intergovernmental Panel on Climate Change (IPCC), Geneva, Switzerland, for kindly providing the permission to use Figure TS.7; Figure 5.9 from IPCC 2005: IPCC Special Report on Carbon Dioxide Capture and Storage, prepared by Working Group III of the IPCC (Metz, B., O. Davidson, H.C. de Coninck, M. Loos, and L. A. Meyer (eds.)). Cambridge University Press, Cambridge, United Kingdom and New York, NY, USA. The authors would like to convey their sincere appreciation to ACS publishers for kindly granting the permission to use Figures 8(a), 10, and 12 from [15].

Conflict of interest

The authors declare no competing financial interest.

Notes/Thanks/Other declarations

The lead author, Dr. Prem Bikkina, would like to express his sincere appreciation for Drs. Jiamin Wan and Tetsu Tokunaga (Lawrence Berkeley National Laboratory, USA), Dr. Stefan Iglauer (Edith Cowan University, Australia), and Dr. Daniel Broseta (Université De Pau Et Des Pays De L'adour, France) for their participation in the scientific discussions with him on the topics related to this chapter.

Author details

Prem Bikkina* and Imran Shaik

*Address all correspondence to: prem.bikkina@okstate.edu

Oklahoma State University, Stillwater, USA

References

[1] Bachu S. Sequestration of CO_2 in geological media: Criteria and approach for site selection in response to climate change. Energy Conversion and Management. 2000;**41**(9):953-970

[2] Oldenburg CM, Pruess K, Benson SM. Process modeling of CO_2 injection into natural gas reservoirs for carbon sequestration and enhanced gas recovery. Energy & Fuels. 2001;**15**(2):293-298

[3] Shaw J, Bachu S. Screening, evaluation, and ranking of oil reservoirs suitable for CO_2-flood EOR and carbon dioxide sequestration. Journal of Canadian Petroleum Technology. 2002;**41**(9):51-61

[4] Bachu S, Adams JJ. Sequestration of CO_2 in geological media in response to climate change: Capacity of deep saline aquifers to sequester CO_2 in solution. Energy Conversion and Management. 2003;**44**(20):3151-3175

[5] Benson SM, Cole DR. CO_2 sequestration in deep sedimentary formations. Elements. 2008;**4**(5):325-331

[6] Haefeli S, Bosi M, Philibert C. Carbon Dioxide Capture and Storage Issues—Accounting and Baselines Under the United Nations Framework Convention on Climate Change (UNFCCC). Paris, France: International Energy Agency; 2004. Available from: http://www/.iea.org/papers/2004/css.pdf

[7] Holloway S. Underground sequestration of carbon dioxide—A viable greenhouse gas mitigation option. Energy. 2005;**30**(11-12):2318-2333

[8] Holtz MH. Optimizing Permanent CO_2 Sequestration in Brine Aquifers: Example from the Upper Frio, Gulf of Mexico. Carbon dioxide sequestration in geological media—State of the science. AAPG Studies in Geology. 2009;**59**:429-437

[9] Akbarabadi M, Piri M. Relative permeability hysteresis and capillary trapping characteristics of supercritical CO_2/brine systems: An experimental study at reservoir conditions. Advances in Water Resources. 2013;**52**:190-206

[10] Rahman T et al. Residual trapping of supercritical CO_2 in oil-wet sandstone. Journal of Colloid and Interface Science. 2016;**469**:63-68

[11] Tokunaga TK et al. Capillary pressure and saturation relations for supercritical CO_2 and brine in sand: High-pressure Pc (Sw) controller/meter measurements and capillary scaling predictions. Water Resources Research. 2013;**49**(8):4566-4579

[12] Wang S, Tokunaga TK. Capillary pressure–saturation relations for supercritical CO_2 and brine in limestone/dolomite sands: Implications for geologic carbon sequestration in carbonate reservoirs. Environmental Science & Technology. 2015;**49**(12):7208-7217

[13] Chalbaud C et al. Interfacial tension measurements and wettability evaluation for geological CO_2 storage. Advances in Water Resources. 2009;**32**(1):98-109

[14] Li Z et al. CO_2 sequestration in depleted oil and gas reservoirs—Caprock characterization and storage capacity. Energy Conversion and Management. 2006;**47**(11-12):1372-1382

[15] Bikkina PK, Shoham O, Uppaluri R. Equilibrated interfacial tension data of the CO_2–water system at high pressures and moderate temperatures. Journal of Chemical & Engineering Data. 2011;**56**(10):3725-3733

[16] Saraji S et al. Wettability of supercritical carbon dioxide/water/quartz systems: Simultaneous measurement of contact angle and interfacial tension at reservoir conditions. Langmuir. 2013;**29**(23):6856-6866

[17] Hough E, Heuer G, Walker J. An improved pendant drop, interfacial tension apparatus and data for carbon dioxide and water. Transactions of the American Institute of Mining and Metallurgical Engineers. 1959;**216**:469-480

[18] Chiquet P et al. CO_2/water interfacial tensions under pressure and temperature conditions of CO_2 geological storage. Energy Conversion and Management. 2007;**48**(3):736-744

[19] Kvamme B et al. Measurements and modelling of interfacial tension for water + carbon dioxide systems at elevated pressures. Computational Materials Science. 2007;**38**(3):506-513

[20] Bachu S, Bennion DB. Interfacial tension between CO_2, freshwater, and brine in the range of pressure from (2 to 27) MPa, temperature from (20 to 125) °C, and water salinity from (0 to 334 000) mg L^{-1}. Journal of Chemical & Engineering Data. 2008;**54**(3):765-775

[21] Shah V et al. Water/acid gas interfacial tensions and their impact on acid gas geological storage. International Journal of Greenhouse Gas Control. 2008;**2**(4):594-604

[22] Aggelopoulos C, Robin M, Vizika O. Interfacial tension between CO_2 and brine (NaCl + $CaCl_2$) at elevated pressures and temperatures: The additive effect of different salts. Advances in Water Resources. 2011;**34**(4):505-511

[23] Espinoza DN, Santamarina JC. Water-CO_2-mineral systems: Interfacial tension, contact angle, and diffusion—Implications to CO_2 geological storage. Water Resources Research. 2010;**46**(7)

[24] Georgiadis A et al. Interfacial tension measurements of the (H_2O+CO_2) system at elevated pressures and temperatures. Journal of Chemical & Engineering Data. 2010;**55**(10): 4168-4175

[25] Shariat A et al. Laboratory measurements of CO_2-H_2O interfacial tension at HP/HT conditions: Implications for CO_2 sequestration in deep aquifers. In: Carbon Management Technology Conference. 2012

[26] Al-Yaseri A et al. N_2 + CO_2 + NaCl brine interfacial tensions and contact angles on quartz at CO_2 storage site conditions in the Gippsland basin, Victoria/Australia. Journal of Petroleum Science and Engineering. 2015;**129**:58-62

[27] Arif M et al. Impact of pressure and temperature on CO_2–brine–mica contact angles and CO_2–brine interfacial tension: Implications for carbon geo-sequestration. Journal of Colloid and Interface Science. 2016;**462**:208-215

[28] Kravanja G, Knez Ž, Hrnčič MK. The effect of argon contamination on interfacial tension, diffusion coefficients and storage capacity in carbon sequestration processes. International Journal of Greenhouse Gas Control. 2018;**71**:142-154

[29] Chun B-S, Wilkinson GT. Interfacial tension in high-pressure carbon dioxide mixtures. Industrial & Engineering Chemistry Research. 1995;**34**(12):4371-4377

[30] Iglauer S et al. Contamination of silica surfaces: Impact on water–CO_2–quartz and glass contact angle measurements. International Journal of Greenhouse Gas Control. 2014;**22**: 325-328

[31] Bikkina PK. Contact angle measurements of CO_2–water–quartz/calcite systems in the perspective of carbon sequestration. International Journal of Greenhouse Gas Control. 2011;**5**(5):1259-1271

[32] Al-Yaseri AZ et al. Receding and advancing (CO_2 + brine + quartz) contact angles as a function of pressure, temperature, surface roughness, salt type and salinity. The Journal of Chemical Thermodynamics. 2016;**93**:416-423

[33] Arif M et al. CO_2 storage in carbonates: Wettability of calcite. International Journal of Greenhouse Gas Control. 2017;**62**:113-121

[34] Wang S, Edwards IM, Clarens AF. Wettability phenomena at the CO_2–brine–mineral interface: implications for geologic carbon sequestration. Environmental Science & Technology. 2012;**47**(1):234-241

[35] Farokhpoor R et al. Wettability behaviour of CO_2 at storage conditions. International Journal of Greenhouse Gas Control. 2013;**12**:18-25

[36] Levine JS et al. Relative permeability experiments of carbon dioxide displacing brine and their implications for carbon sequestration. Environmental Science & Technology. 2013;**48**(1):811-818

[37] Andrew M, Bijeljic B, Blunt MJ. Pore-scale contact angle measurements at reservoir conditions using X-ray microtomography. Advances in Water Resources. 2014;**68**:24-31

[38] Sarmadivaleh M, Al-Yaseri AZ, Iglauer S. Influence of temperature and pressure on quartz–water–CO_2 contact angle and CO_2–water interfacial tension. Journal of Colloid and Interface Science. 2015;**441**:59-64

[39] Peters EJ. Advanced Petrophysics: Dispersion, Interfacial Phenomena. Vol. 2. Austin, TX: Live Oak Book Company; 2012

[40] Broseta D, Tonnet N, Shah V. Are rocks still water-wet in the presence of dense CO_2 or H_2S? Geofluids. 2012;**12**(4):280-294

[41] Jung J-W, Wan J. Supercritical CO_2 and ionic strength effects on wettability of silica surfaces: Equilibrium contact angle measurements. Energy & Fuels. 2012;**26**(9):6053-6059

[42] Saraji S, Piri M, Goual L. The effects of SO_2 contamination, brine salinity, pressure, and temperature on dynamic contact angles and interfacial tension of supercritical CO_2/brine/quartz systems. International Journal of Greenhouse Gas Control. 2014;**28**:147-155

[43] Peng D-Y, Robinson DB. A new two-constant equation of state. Industrial and Engineering Chemistry Fundamentals. 1976;**15**(1):59-64

[44] Søreide I, Whitson CH. Peng-Robinson predictions for hydrocarbons, CO_2, N_2, and H_2S with pure water and NaCl brine. Fluid Phase Equilibria. 1992;**77**:217-240

[45] Rowe AM Jr, Chou JC. Pressure-volume-temperature-concentration relation of aqueous sodium chloride solutions. Journal of Chemical and Engineering Data. 1970;**15**(1):61-66

[46] Perry RH, Green DW. Perry's Chemical Engineering Handbook. 7th ed. New York: McGraw-Hill; 1997

[47] McCutcheon SC, Martin JL, Barnwell TO Jr. Water quality. In: Handbook of Hydrology. Vol. 11. 1993. p. 73

[48] Duan Z, Sun R. An improved model calculating CO_2 solubility in pure water and aqueous NaCl solutions from 273 to 533 K and from 0 to 2000 bar. Chemical Geology. 2003;**193**(3-4):257-271

[49] Hebach A, Oberhof A, Dahmen N. Density of water + carbon dioxide at elevated pressures: measurements and correlation. Journal of Chemical & Engineering Data. 2004;**49**(4): 950-953

[50] Spycher N, Pruess K, Ennis-King J. CO_2-H_2O mixtures in the geological sequestration of CO_2. I. Assessment and calculation of mutual solubilities from 12 to 100 C and up to 600 bar. Geochimica et Cosmochimica Acta. 2003;**67**(16):3015-3031

[51] Lecture Notes—Silica Polymorphs. [Cited: June 3, 2018]. Available from: http://www.science.smith.edu/geosciences/min_jb/SilicaPolymorphs.pdf

[52] Carbonates. [Cited: June 3, 2018]. Available from: http://www.minerals.net/mineral_glossary/carbonates.aspx

[53] Mica group. [Cited: June 3, 2018]. Available from: http://www.minerals.net/mineral_glossary/mica_group.aspx

[54] Wan J, Kim Y, Tokunaga TK. Contact angle measurement ambiguity in supercritical CO_2–water–mineral systems: Mica as an example. International Journal of Greenhouse Gas Control. 2014;**31**:128-137

[55] Chiquet P, Broseta D, Thibeau S. Wettability alteration of caprock minerals by carbon dioxide. Geofluids. 2007;**7**(2):112-122

[56] Eske LD, Galipeau DW. Characterization of SiO_2 surface treatments using AFM, contact angles and a novel dewpoint technique. Colloids and Surfaces A: Physicochemical and Engineering Aspects. 1999;**154**(1-2):33-51

[57] Alam AU. Surface Analysis of Materials for Direct Wafer Bonding. 2014

[58] Horn R, Smith D, Haller W. Surface forces and viscosity of water measured between silica sheets. Chemical Physics Letters. 1989;**162**(4-5):404-408

[59] Suni T et al. Effects of plasma activation on hydrophilic bonding of Si and SiO_2. Journal of the Electrochemical Society. 2002;**149**(6):G348-G351

[60] Lamb RN, Furlong DN. Controlled wettability of quartz surfaces. Journal of the Chemical Society, Faraday Transactions 1: Physical Chemistry in Condensed Phases. 1982;**78**(1):61-73

[61] Bolis V et al. Hydrophilic and hydrophobic sites on dehydrated crystalline and amorphous silicas. Journal of the Chemical Society, Faraday Transactions. 1991;**87**(3):497-505

[62] Sneh O, George SM. Thermal stability of hydroxyl groups on a well-defined silica surface. The Journal of Physical Chemistry. 1995;**99**(13):4639-4647

[63] Zhao L et al. Molecular dynamics investigation of the various atomic force contributions to the interfacial tension at the supercritical CO_2–water interface. The Journal of Physical Chemistry B. 2011;**115**(19):6076-6087

[64] Iglauer S, Mathew M, Bresme F. Molecular dynamics computations of brine–CO_2 interfacial tensions and brine–CO_2–quartz contact angles and their effects on structural and residual trapping mechanisms in carbon geo-sequestration. Journal of Colloid and Interface Science. 2012;**386**(1):405-414

[65] Nielsen LC, Bourg IC, Sposito G. Predicting CO_2–water interfacial tension under pressure and temperature conditions of geologic CO_2 storage. Geochimica et Cosmochimica Acta. 2012;**81**:28-38

[66] Liu Y et al. Simulations of vapor–liquid phase equilibrium and interfacial tension in the CO_2–H_2O–NaCl system. AICHE Journal. 2013;**59**(9):3514-3522

[67] McCaughan J, Iglauer S, Bresme F. Molecular dynamics simulation of water/CO_2-quartz interfacial properties: Application to subsurface gas injection. Energy Procedia. 2013;**37**:5387-5402

[68] Tenney CM, Cygan RT. Molecular simulation of carbon dioxide, brine, and clay mineral interactions and determination of contact angles. Environmental Science & Technology. 2014;**48**(3):2035-2042

[69] Chen C et al. Water contact angles on quartz surfaces under supercritical CO_2 sequestration conditions: Experimental and molecular dynamics simulation studies. International Journal of Greenhouse Gas Control. 2015;**42**:655-665

[70] Liu S, Yang X, Qin Y. Molecular dynamics simulation of wetting behavior at CO_2/water/solid interfaces. Chinese Science Bulletin. 2010;**55**(21):2252-2257

[71] Van Beest B, Kramer GJ, Van Santen R. Force fields for silicas and aluminophosphates based on ab initio calculations. Physical Review Letters. 1990;**64**(16):1955

[72] Hebach A et al. Interfacial tension at elevated pressures measurements and correlations in the water + carbon dioxide system. Journal of Chemical & Engineering Data. 2002;**47**(6):1540-1546

[73] Marmur A et al. Contact angles and wettability: Towards common and accurate terminology. Surface Innovations. 2017;**5**(1):3-8

[74] Jafari M, Jung J. Variation of contact angles in Brine/CO_2/Mica system considering short-term geological CO_2 sequestration condition. Geofluids. 2018;**2018**

[75] Tripp C, Combes J. Chemical modification of metal oxide surfaces in supercritical CO_2: The interaction of supercritical CO_2 with the adsorbed water layer and the surface hydroxyl groups of a silica surface. Langmuir. 1998;**14**(26):7348-7352

[76] Kim Y et al. Dewetting of silica surfaces upon reactions with supercritical CO_2 and brine: Pore-scale studies in micromodels. Environmental Science & Technology. 2012;**46**(7): 4228-4235

[77] Shi L et al. Wetting and evaporation behaviors of water–ethanol sessile drops on PTFE surfaces. Surface and Interface Analysis. 2009;**41**(12-13):951-955

[78] Anantharaju N, Panchagnula M, Neti S. Evaporating drops on patterned surfaces: Transition from pinned to moving triple line. Journal of Colloid and Interface Science. 2009;**337**(1):176-182

[79] Bikkina PK. Reply to the comments on "Contact angle measurements of CO_2–water–quartz/calcite systems in the perspective of carbon sequestration". International Journal of Greenhouse Gas Control. 2012;**7**:263-264

[80] Al-Yaseri AZ et al. Dependence of quartz wettability on fluid density. Geophysical Research Letters. 2016;**43**(8):3771-3776

[81] AlRatrout A et al. Automatic measurement of contact angle in pore-space images. Advances in Water Resources. 2017;**109**:158-169